2016

A New Flow Map and Flow Characterization of Condensation in Smooth Round Tube from Superheated Vapor

Jiange Xiao
ACRC, the University of Illinois, jxiao10@illinois.edu

Pega Hrnjak
pega@illinois.edu

A New Flow Map and Flow Characterization of Condensation in Smooth Round Tube from Superheated Vapor

Jiange XIAO[1], Pega HRNJAK[1,2]*

[1]University of Illinois at Urbana-Champaign,

Department of Science and Engineering,

Urbana, IL, USA

Jxiao10@illinois.edu, pega@illinois.edu

[2]Creative Thermal Solutions,

Urbana, IL, USA

* Corresponding Author

ABSTRACT

Flow characterization of R134a condensing in a horizontal smooth round tube with 6.1 mm inner diameter is investigated in this study. The paper presents flow visualization and liquid film thickness measurement with mass flux from 50 to 200 kg m^{-2} s^{-1} and heat flux from 5 to 15 kW m^{-2}, showing the effect of mass flux and heat flux on the onset of condensation, flow regime, film distribution and void fraction. All the measurement is taken at constant pressure of 1.319 MPa, which corresponds to a saturation temperature of 50 ^{o}C. The result of flow visualization reveals that the condensation always starts in the bulk superheated (SH) region, as annular flow and the flow regime is strongly affected by mass flow, not heat flux. Based on the flow visualization in the condensing superheated (CSH) region, a new diabatic flow map is proposed to better represent the physics and predict flow regimes in CSH region. A film thickness measurement technique for round tube refined from critical angle method is described and calibrated. The calibration and comparison between the film thickness measurement result and flow visualization shows that the refined critical angle method is able to accurately describe the film distribution inside the tube. The film thickness measurement demonstrates that void fraction drops below one in the SH region, which is not taken into account for most conventional void fraction models. In addition, the void fraction measurement illustrates that mass flux has greater effect on slip ratio than heat flux. Besides, having film distribution information provides an opportunity to more objectively determine the flow regime and develop a more mechanistic model by utilizing the film geometry inside of the tube.

1. INTRODUCTION

Over the years, many researcher have been looking at the subject of condensation. A large number of correlations have been built to predict fluid properties, flow regime, void fraction, pressure drop and heat transfer coefficient (HTC). The improvements of those correlations are usually based on a deeper and better understanding of the process and sometimes larger data base. For in-tube condensation in a heat exchanger, the existence of condensation in the SH region is described by Kondo and Hrnjak (2011a, 2011b, 2012) and Agarwal and Hrnjak (2013) through measurement of HTC and pressure drop in the SH region. The transition behavior of HTC and pressure drop in the CSH region is considered as an indirect indication of condensation in superheated region which deviates reality from existing correlations. Meyer and Hrnjak (2014) further proved the existence of liquid film in superheated region from flow visualization and film thickness measurement of R134a in one working condition. These studies confirmed that condensation can happen in superheated region, yet the physics behind the heat transfer and pressure drop mechanism needs to be better explained. Moreover, there is still no prediction regarding the flow regimes in the CSH region, and little discussion about the film distribution in early stages of condensation. In order to address these issues and better understand the reasons behind them, flow visualization, film thickness and heat transfer measurement were performed simultaneously at different working conditions for the purpose of comparison. This paper focuses on the flow visualization and film thickness measurement. The visualization of flow studies the effect of working conditions on the flow characters, including the onset of condensation and flow regime with emphasis in the CSH region. The film thickness measurement is refined from previous experimental method and carefully calibrated. It quantitatively supports the visualization by giving void fractions and film distribution along the tube circumference.

2. EXPERIMENT DESCRIPTION

2.1 Experimental facility schematic drawing

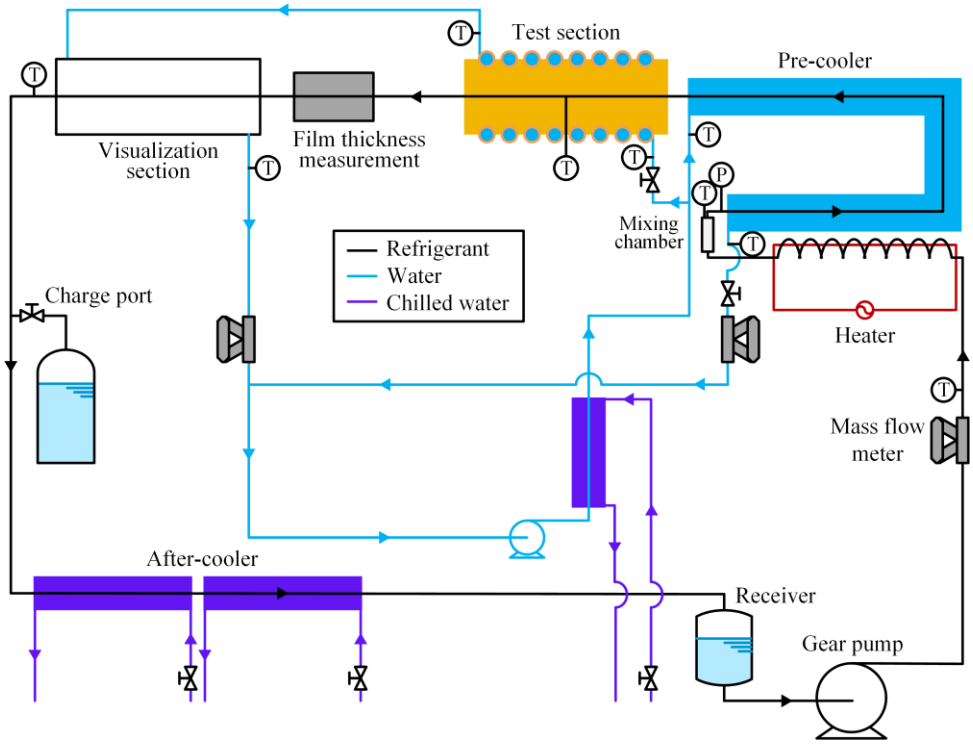

Figure 1: Schematic drawing of experimental facility (Meyer and Hrnjak, 2014)

2.2 Film thickness measurement section

The film thickness measurement is based on the principle proposed by Hurlburt and Newell (1996) and refined by Shedd and Newell (1998). A detailed application and calibration of this method on oil was also described by Jiu and Hrnjak (2016). With this method, a focused light beam is shined on the surface of duct tape wrapped around a glass tube with 6 mm inner diameter and 10 mm outer diameter. The light is assumed to be diffused uniformly in each direction. The light appearing on the tape is the brightest at the spot where light is shined on. Generally speaking, the further away from the source, the lower the brightness of light is. However, at some point when the incident angle reached critical angle for total reflection, since all of the light is reflected, there is a sudden increase of brightness. The location of the jump in brightness forms an ellipse whose size is dependent on the thickness of the liquid film layer inside the tube. The major diameter is chosen to be related to the film thickness because the major diameter denotes the axial direction of the glass tube where there is no curvature effect of the cylindrical glass tube. Hence the optical model can be simplified as a flat plate. The ellipse is caught on a web camera and a correlation is built to convert major diameter to film thickness. The major diameter is related to film thickness via an optical model described as Equation (1). To get the film distribution around the tube, four photos of ellipse are taken at each angle of 0°, 60°, 90°, 135°, 180°, 225°, 270°, and 300° clockwise from the bottom of the tube. The film thicknesses calculated at each angle are then averaged.

$$Major\ Diameter = 4 * (\frac{\delta_{film}}{\sqrt{n_r^2 - 1}} + \frac{\delta_{wall}}{\sqrt{n_w^2 - 1}}) \quad (1)$$

2.3 Visualization section

The visualization section is a coaxial heat exchanger made out of glass. The heat exchanger is around 20 cm long. The refrigerant flows through a tube with 6 mm inner diameter and 12 mm outer diameter. The secondary fluid is water taken directly out of the outlet of test section to better simulate the conditions in test section. The inner diameter of the outer tube is 17 mm and outer diameter is 20 mm. High-speed video is recorded at 1000 frames per second and the resolution was 512 by 512 pixels. The bulk enthalpy of refrigerant is taken as the inlet enthalpy of visualization section because the change of quality in the visualization section is generally less than 0.1.

2.4 Critical angle method calibration

Figure 2 shows the schematic drawing of the critical angle method calibration facility. The calibration is performed to relate major diameter and film thickness in order to make the measurement more accurate. The calibration of the optical film thickness measurement is done by simultaneously measuring the thickness of a liquid film in a half glass tube using two different methods: the critical angle method and the contact needle method. The glass tube has the same dimensions and material as that used for experiment. The contact needle method uses a micrometer with a needle probe to detect the level of liquid film, which is considered accurate but intrusive. HFE 7100 is used here as the calibration fluid due to its similar properties with refrigerants, and it remaining liquid under room temperature and atmospheric pressure. The film thickness measured from the critical angle method is then compared with that measured from the contact needle method. The result using the optical model agrees with the contact needle method within 10 percent discrepancy, which is shown in Figure 3.

Because of the limitations in the contact needle method, the calibration range is actually larger than most of the experimental data, implying that the actual relative uncertainty, especially for the smaller thickness might be larger than that from the calibration. The limitation in the critical angle method will be discussed in the following sections.

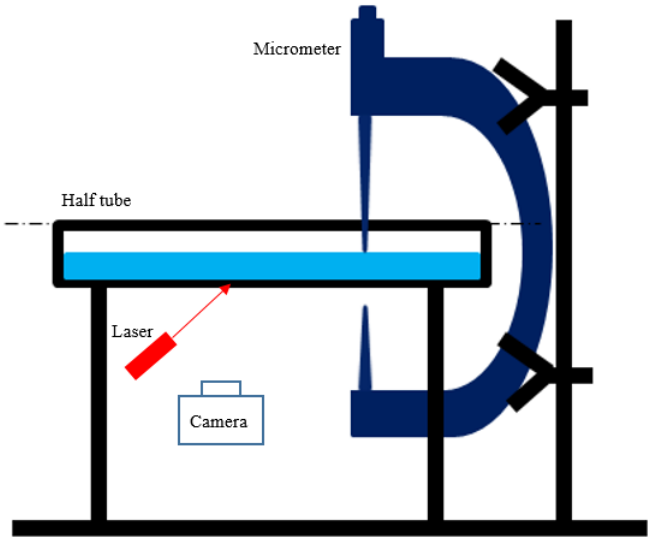

Figure 2: Schematic drawing of critical angle method calibration facility

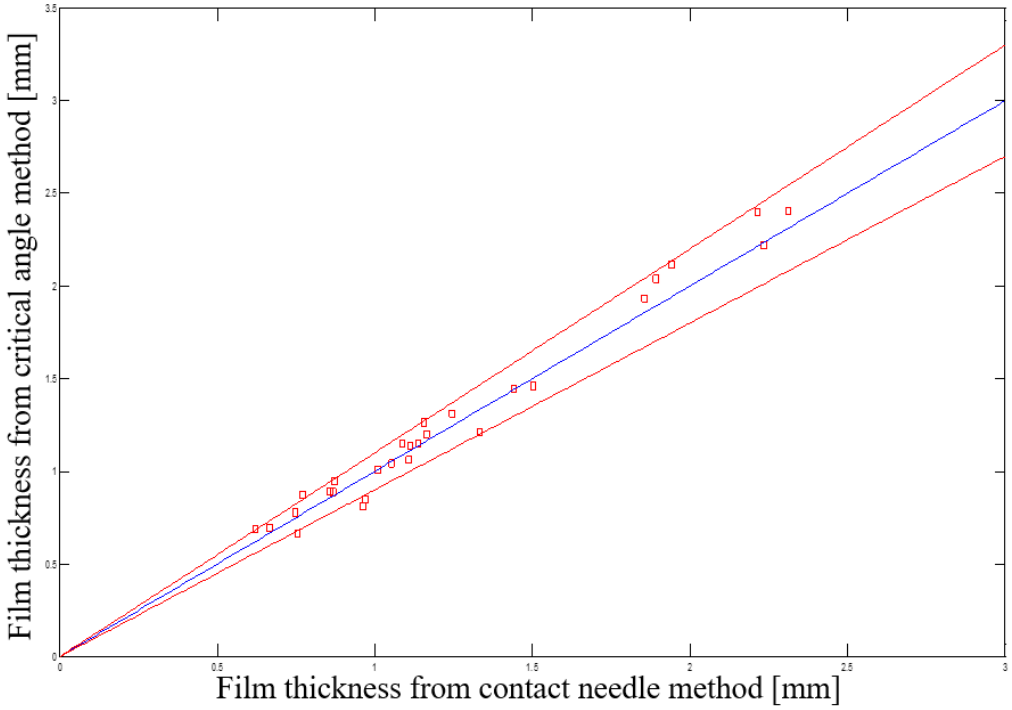

Figure 3: Film thickness measurement from critical angle method vs contact needle method

3. RESULTS AND DISCUSSIONS

3.1 Flow visualization

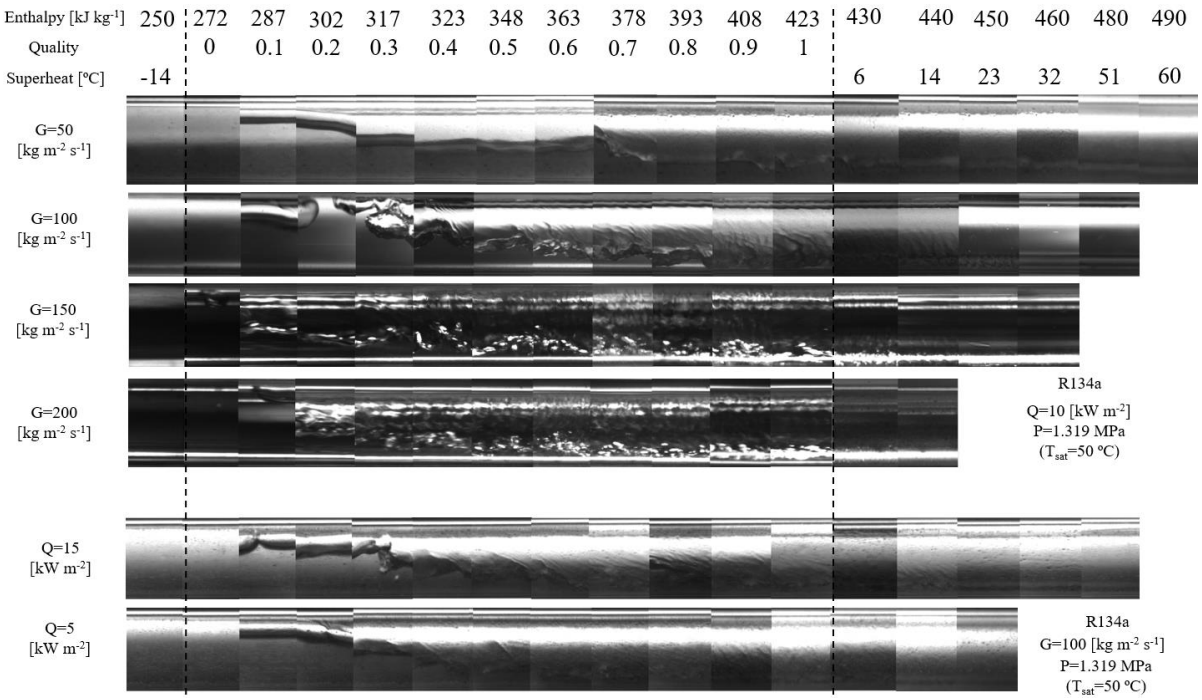

Figure 4: Pictures from high speed videos of condensation under different working conditions

From the visualization, the onset of condensation is always in the SH region which denotes the beginning of the CSH region but the location of onset varies with different working conditions. When heat flux is fixed, the higher the mass flux, the later (lower enthalpy) the condensation happens; when mass flux is fixed, the higher the heat flux, the earlier (higher enthalpy) the condensation happens. This is because when the mass flux is higher, the single phase HTC is higher. To maintain the same heat flux, the required temperature difference is smaller, meaning the wall temperature will be higher at the same enthalpy and the wall temperature drops below saturation at a lower enthalpy. To summarize, the properties of the fluid and working conditions dictate the onset of condensation. As soon as the wall temperature drops below saturation temperature, there will be liquid refrigerant on the tube wall, which always happens before bulk quality drops to one due to the temperature gradient required for heat transfer to happen.

When the wall temperature drops below saturation temperature, condensation starts and liquid film forms. Due to the shear and gravitational effects, the film will be dragged downstream and pulled downwards simultaneously. At the early stages of condensation, liquid film is very thin, hence the shear force and surface tension prevails against gravity, meaning the flow regime has to be annular. It is only after the film becomes thicker that gravitational force starts to dominate. From the visualization, the condensation always starts in annular flow regime for each working condition and changes to wavy or stratified flow after the film grows for a while. The duration of being in the annular flow regime depends on the working condition. The higher the mass flux, the more portion of condensation process stays in the annular flow regime because the shear between liquid and vapor is stronger and film thickness is thinner which is confirmed by film thickness measurement. In summary, the early stages of condensation have to be annular and the duration of being annular flow depends on mass flux.

From the visualization, it can be seen that flow regime is strongly dependent on mass flux. The higher the mass flux, the larger the portion of the condensation process in annular regime, and smaller the portion in the stratified flow regime. On the contrary, for lower mass flux, the larger portion of the condensation process is in the stratified regime. Meanwhile, the film thickness is thinner at the same enthalpy for higher mass flux since the condensation rate (heat flux) is the same for each different mass flux. Higher mass flux creates greater shear at interface and pulls more liquid away. Moreover, higher flux creates better mixing. From the visualization, the higher the mass flux, the more liquid is entrained into the vapor core. Unlike mass flux, heat flux has little effect on flow regime. At the same

mass flux, all three cases with different heat flux but same mass flux of 100 kg m^{-2} displayed almost identical flow regime at each enthalpy. Therefore, the flow regime is dependent on mass flux but not heat flux.

If the result of flow visualization is compared with conventional flow regime maps for condensation, two major disagreements can be noticed. Firstly, the conventional flow regime maps are based on the assumption of equilibrium that no temperature gradient is present in the TP region. Hence they only predict flow regime from quality one to quality zero. The reality, however, is that condensation happens before quality one as long as there is heat transfer and the conventional flow regime map cannot provide information in the CSH region. Secondly, the predicted early-stage flow regime of condensation is not exclusively annular from the conventional flow map, which is physically impossible from the discussion above and disagrees with the visualization results.

To address the above-mentioned disagreements, a new flow map is proposed below. It is modified from a flow map by Hajal, Thome and Cavallini (2003). Figure 5 shows that the new flow map satisfactorily predicts the flow regime across the entire condensation process including flow regimes in the CSH region and starting exclusively as annular flow. For the new flow map, "superficial quality" is defined by taking the enthalpy of condensation onset as 1 and end of condensation as zero. The rest of the superficial quality is then determined by the specific enthalpy just as the conventional definition of "quality". To draw the new flow map, follow the method proposed by Hajal et al. with the following modifications:

1) Define enthalpy at the onset of condensation to be superficial quality one. Keep enthalpy of thermodynamic quality zero as superficial quality zero. Adjust each enthalpy to its superficial quality and use the superficial quality just as it is thermodynamic quality in the equations.
2) Skip the process of finding minimum G_{mist} and use the value as calculated for higher superficial quality instead of using minimum G_{mist} as stated in the paper.
3) Changing the "$+ 50 - 75\exp(\cdots)$" in G_{wavy} into"$+ 100 - 50\exp(\cdots)$".
4) After finding $G_{wavy,min}$, calculate new G_{wavy} when superficial quality is larger than that of $G_{wavy,min}$ using $G_{wavy} = G_{wavy,min}(1-x)^{0.5}$, making G_{wavy} approach zero as superficial quality approaches one.
5) Changing the last term in equation for G_{strat} from $(+20x)$ to $(+20 - 40x^2)$, making G_{strat} approach zero as superficial quality approaches one.

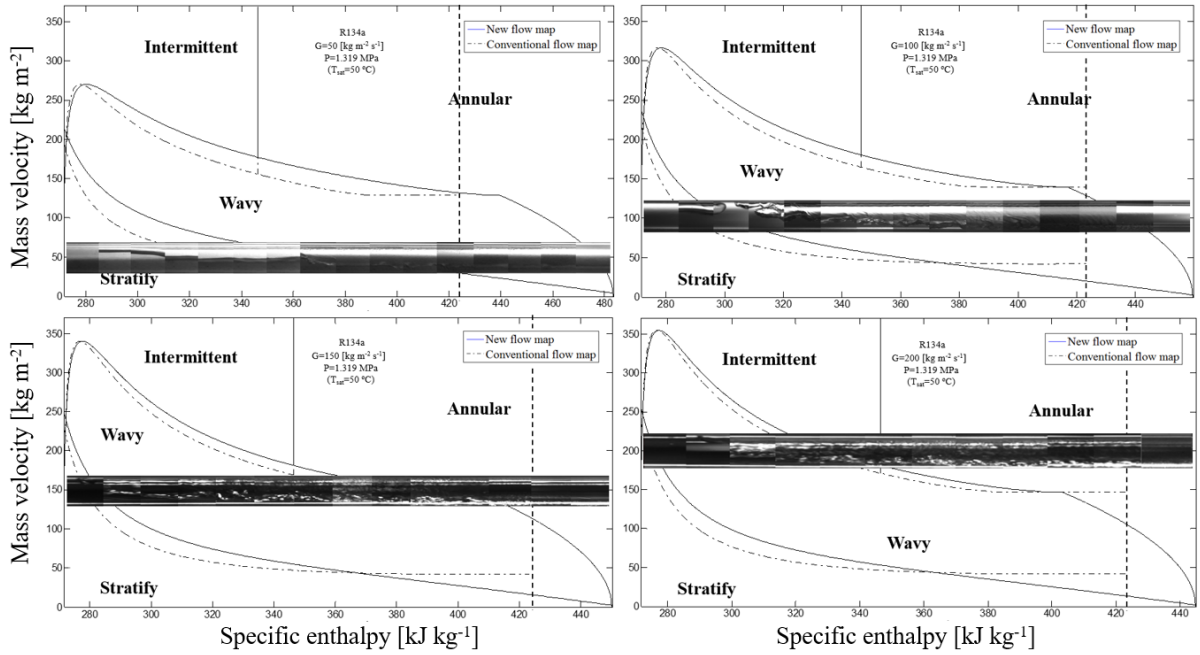

Figure 5: Flow visualizations vs conventional and new flow map at saturation pressure of 1319 kPa (T_{sat}=50 °C) and different mass velocities

3.2 Film thickness measurement

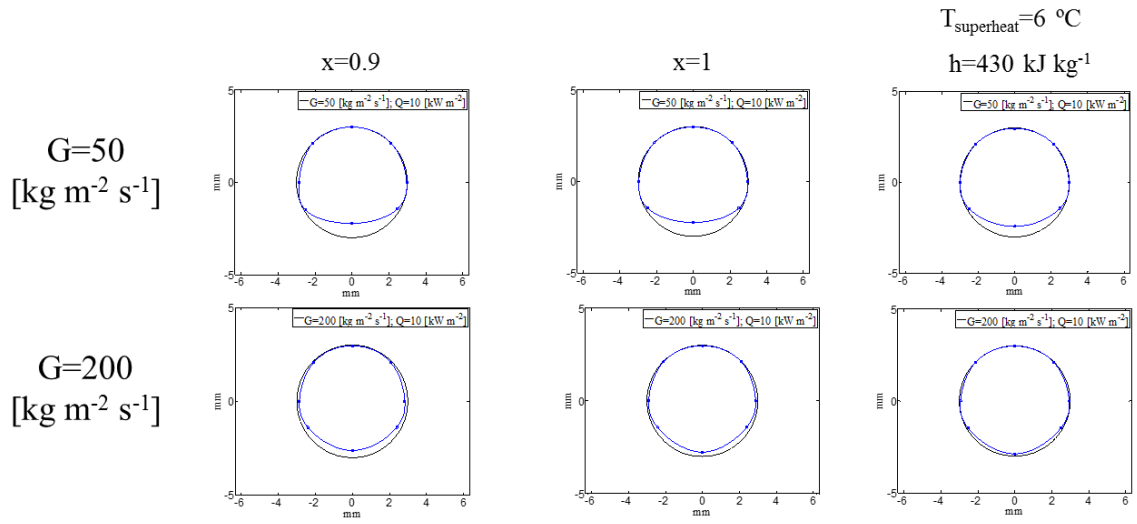

Figure 6: Illustration of film thickness measurement results

Film distribution is measured for the entrance stages of each working condition. Figure 6 serves as an illustration of liquid-film distributions. Firstly, all measurements of film thickness show the existence of liquid film in the CSH region. Also, the onset of condensation determined from the film thickness measurement agrees with that from the flow visualization. Additionally, if film distribution is compared with a fixed mass flux, as condensation proceeds, liquid film grows thicker, and more liquid tends to be drawn to the bottom of the tube when mass flux is lower because the shear force is smaller. If the distribution is compared with different mass flux, it can be seen that the film is thinner and more uniform as mass flux increases. Since film thickness is directly related to thermal resistance and flow regime, the film distribution could potentially act as the indicator of HTC and flow map.

Even though the critical angle method has lots of advantages such as non-intrusive, low cost and fast temporal response, the film thickness measurement has its limits. The range of film thickness this method can measure is very limited. First, the accuracy of this method relies on the accuracy of image recording and processing. If the film thickness is too small, the system error tends to yield huge relative uncertainty, making the result less trustful. Also, the interface between wall and liquid refrigerant creates a second ellipse from its total reflection. There is a chance for those two ellipses to be too close to distinguish one from the other. Moreover, wavy structure would make the measurement unstable. In this study, four pictures are taken at the same condition and the average value is considered the representative of film thickness. However, if the flow becomes too wavy, the measurement might not physically make sense. Therefore, the range of film thickness in this study is selected to be 0 to 0.8 mm.

3.3 Void fraction

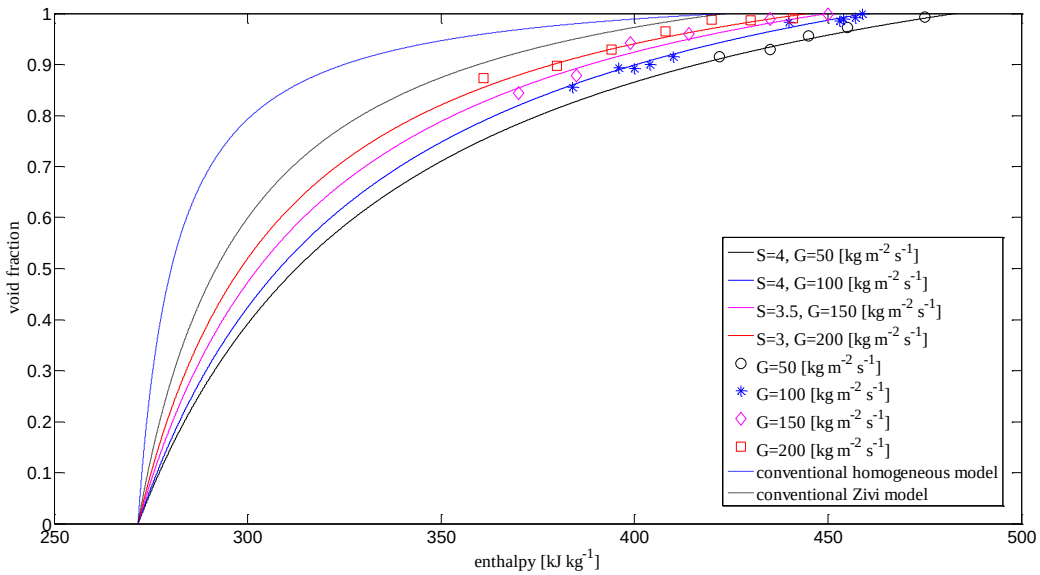

Figure 7: Comparison of void fractions with same heat flux and different mass fluxes

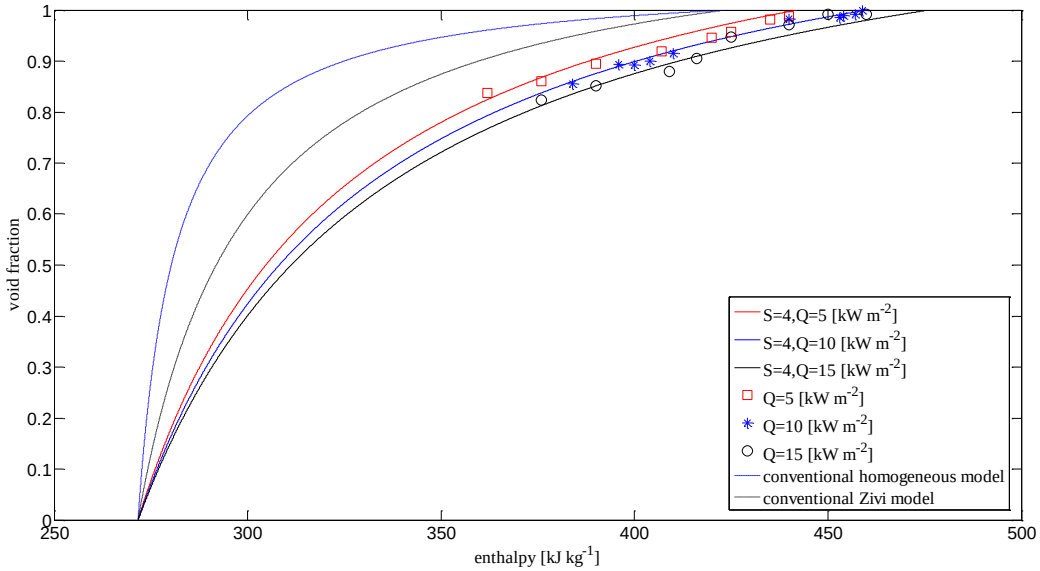

Figure 8: Comparison of void fractions with same mass flux and different heat fluxes

Figure 7 and Figure 8 are the void fraction determined from film thickness measurement compared with original and modified void fraction models. Similar to conventional flow maps, conventional void fraction models predict only from quality one to zero. The experimental data suggests void fraction falls below one before quality one which is not included in the models. To address this issue, same measure is taken as flow map where the onset of condensation is set to be superficial quality one and superficial qualities are assigned according to the enthalpies. Slip ratios are assigned to fit the experimental data, and it shows that mass flux changes the slip ratio while heat flux does not. In detail, Figure 7 shows that instead of being constant, slip ratio decreases when mass flux increases. Figure 8 shows that even though the void fractions are not the same for different heat fluxes, the slip ratio is not

affected by heat flux. Therefore, void fraction depends on both the heat flux and mass flux. While heat flux only affects the onset of condensation, mass flux affects both onset of condensation and slip ratio. This suggests that a drift flux model should be considered a better representation of the physics in the future development of void fraction models.

4. CONCLUSIONS

The two-phase flow during condensation of R134a is characterized in this study. From the flow visualization, it can be seen that the CSH region always exists and the onset of condensation depends on both heat flux and mass flux. Based on the observation and film thickness measurement, a new flow map is proposed to predict flow regimes during the entire condensation process. Film thickness measurement demonstrates that with higher mass flux the film is more evenly distributed and thinner. The comparison between void fraction models and experimental data shows that a drift flux model is very promising compared to models with fixed slip ratios.

NOMENCLATURE

SH	Superheated	
CSH	Condensing superheated	
HTC	Heat transfer coefficient	($W\ m^{-2}\ K^{-1}$)
δ	Thickness	(m)
n	refractive index	
T	Temperature	(^oC)
P	Pressure	(Pa)
G	Mass flux	($kg\ m^{-2}$)
Q	Heat flux	($kW\ m^{-2}$)
x	Quality	
S	Slip ratio	

Subscripts

r	Refrigerant
sat	Saturated
w	Wall
f	Film

REFERENCES

Agarwal, R., Hrnjak, P., 2015, Condensation in two phase and desuperheating zone for R1234ze(E), R134a and R32 in horizontal smooth tubes, *Int. J. Refrigeration*, vol. 50, p. 172-183.

El Hajal, J., Thome, J.R., Cavallini, A., 2003, Condensation in horizontal tubes, part 1: two- phase flow pattern map,"*Int. J. Heat Mass Transfer*, vol. 46, no. 18, p. 3349-3363.

Hurlburt, E. T., Newell, T. A., 1996, Optical measurement of liquid film thickness and wave velocity in liquid film flows, *Experiments in Fluids*, vol. 21, p. 357-362.

Kondou, C., Hrnjak, P., 2011a, Heat rejection from R744 flow under uniform temperature cooling in a horizontal smooth tube around the critical point, *Int. J. Refrigeration*, vol. 34, no. 3, p. 719-731.

Kondou, C., Hrnjak, P., 2011b, Heat rejection in condensers close to critical point-desuperheating, condensation in superheated region and condensation of two phase fluid, *Int. Conf. Heat Trans. Fluid Mech. and Thermodynamics*, Mauritius.

Kondou, C., Hrnjak, P., 2012, Condensation from superheated vapor flow of R744 and R410A at subcritical pressures in a horizontal smooth tube, *Int. J. Heat Mass Transfer,* vol. 55, p. 2779-2791.

Meyer, M., Hrnjak, P., 2014, Pressure Drop in Condensing Superheated Zone *Proc. International Refrigeration Conference*, West Lafayette, IN, USA.

Shedd, T. A., Newell, T. A., 1998, Automated optical liquid film thickness measurement method, *Review of Scientific Instruments*, vol. 69, no. 12, p. 4205-4213.

Xu, J., Hrnjak, P., 2016, Refrigerant-Oil Flow at the Compressor Discharge, *SAE Technical Paper, 2016-01-0247.*

ACKNOWLEDGEMENT

The authors thankfully acknowledge the support provided by the Air Conditioning and Refrigeration Center at the University of Illinois at Urbana-Champaign.